16th Australasian Fluid Mechanics Conference
Crown Plaza, Gold Coast, Australia
2-7 December 2007

# Correcting cold wire measurements in isotropic turbulence with a DNS database

**P. Burattini, M. Kinet, D. Carati, and B. Knaepen**

Physique Statistique et des Plasmas
Université Libre de Bruxelles, B-1050 Brussels, BELGIUM

**Abstract**

We estimate the effect of the finite spatial resolution of a cold wire for scalar measurements, using a database from direct numerical simulations (DNS). These are for homogeneous isotropic turbulence at low Taylor-microscale Reynolds number ($\simeq 42$) and Schmidt number unity. Correction factors for the scalar variance, scalar mean dissipation rate, and mixed velocity-scalar derivative skewness are evaluated, for a sensor length of up to 15 times the Batchelor length scale. The largest attenuation effect is found on the dissipation rate, followed by the scalar variance. The mixed skewness, which is affected the least, is overestimated.

## Introduction

Measurements in turbulence can be seriously degraded, if the spatial resolution of the probe is inadequate. For example, small-scale quantities such as the dissipation rates of velocity and scalar fluctuations are underestimated, when the size of the sensor is significantly larger than the dissipative length scales. These are the Kolmogorov length scale $\eta$ ($=\nu^{3/4}\varepsilon^{-1/4}$, where $\nu$ is the kinematic viscosity and $\varepsilon$ is the mean energy dissipation rate) for the velocity, and the Batchelor length scale $\eta_B$ ($=\eta Sc^{-1/2}$, where $Sc=\nu/\nu_\theta$ is the Schmidt number and $\nu_\theta$ is the scalar diffusivity) for the scalar. As the Reynolds number increases, $\eta$ and $\eta_B$ become smaller, and the resolution worsens, for a given probe size. Although numerical simulations of turbulence are not immune from resolution issues, the situation improves, as the computing resources increase. On the contrary, the size of a typical hot/cold wire has not changed for decades, and therefore procedures that compensate for the probe attenuation remain topical.

Wyngaard [15, 16] proposed a spectral method for correcting hot/cold wire measurements in isotropic turbulence. Given an analytical three-dimensional (3D) spectrum for the kinetic energy or the scalar variance, the one-dimensional (1D) spectrum is derived through isotropic relations, so that the averaging effect due to the length of the sensor can be estimated and corrected. Wyngaard's approach is currently applied in measuring with these instruments [6, 5], which are still unsurpassed for the experimental analysis of small-scale turbulence at high temporal and spatial resolution. A slightly different procedure consists in using an experimental expression for the 1D spectrum measured at low Reynolds numbers, so that it is fully resolved [1]. Mi and Nathan [10] simulated the effect of poor temporal resolution by digitally undersampling the scalar signal, which was acquired in the far-field of a jet. Although they found close agreement with estimates of underresolved scalar measurements from the literature, they noted large differences with respect to Wyngaard's prediction. To date, there is no direct validation of Wyngaard's method in isotropic scalar turbulence. Nevertheless, providing such validation is important, because cold wires are still widely used for scalar measurements.

Fully resolved simulations of homogeneous isotropic turbulence make it possible to test directly the averaging effect due to the sensor size. Filtered or 'measured' turbulent quantities can be estimated by averaging locally the instantaneous (velocity or scalar) field across an ideal wire, e.g. [3, 13]. In the present work, we use a DNS database of isotropic scalar turbulence to study the effect of the probe resolution. Starting from the original fields, filtered surrogates are generated and, from these, correction factors for the scalar variance, mean dissipation rate, and mixed velocity-scalar derivative skewness are estimated. This latter quantity has never been considered in the literature from the viewpoint of resolution corrections. The mixed skewness is related to the scalar transfer, and its value is often quoted to show that scalar turbulence is fully developed [2, 4].

## Analysis of the Attenuation

The present analysis applies to an idealised probe for scalar measurement (e.g. temperature), since it is assumed that the sensitivity of the wire is uniform over its length and is not affected by velocity fluctuations. Further, the probe does not interfere (aerodynamically or thermally) with the flow. With these hypotheses, the filtering effect due to the wire finite size can be readily expressed in physical space. Consider a sensor of length $\ell$, parallel to the $x_2$-direction, and measuring the scalar value in the $x_1$-direction, figure 1. In the experiment, the $x_1$ axis is in the direction of the mean flow. The averaging over $\ell$ of the true scalar field $\theta$ is given by the convolution integral

$$\theta^*(x_1,x_2,x_3;\ell)=\int_{-\ell/2}^{\ell/2} f\left(x_2-x_2'\right)\theta\left(x_1,x_2',x_3\right)dx_2', \qquad (1)$$

where $f$ is the filtering kernel and $x_2'$ is a dummy integration variable (hereafter, the asterisk denotes a filtered quantity). The hypothesis of uniform sensitivity translates into $f\left(x_2-x_2'\right)$ being equal to 1 for $\left|x_2-x_2'\right|\le \ell/2$, and 0 otherwise (the rectangular step function). In spectral space, (1) becomes

$$\hat{\theta}^*(k_1,k_2,k_3;\ell)=\hat{f}(k_2;\ell)\,\hat{\theta}(k_1,k_2,k_3) \qquad (2)$$

(the hat indicates the transformed variables), where the transform of the filtering kernel, or sensitivity, is

$$\hat{f}(k_2;\ell)=\frac{\sin(k_2\ell/2)}{(k_2\ell/2)}, \qquad \hat{f}(0)=1. \qquad (3)$$

As customary, we introduce the scalar power spectrum

$$\phi_\theta(\mathbf{k})=\phi_\theta(k_1,k_2,k_3)=\left|\hat{\theta}(k_1,k_2,k_3)\right|^2, \qquad (4)$$

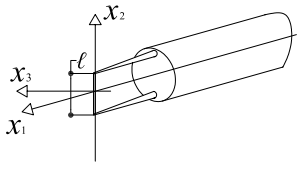


Figure 1: Sketch of the cold wire with coordinate system.

(where $\mathbf{k}$ is the wavenumber vector), related to the 3D spectrum function $E_\theta(k)$ — or simply 3D spectrum — by

$$E_\theta(k) = \int_S \phi_\theta(\mathbf{k})\, dS(k). \tag{5}$$

The integral is carried out over thin spherical shells $S$ centred at $k$, the wavenumber magnitude. Since in isotropic turbulence there is no directional dependence, one has

$$E_\theta(k) = 4\pi k^2 \phi_\theta(k). \tag{6}$$

The true (i.e. unfiltered) 1D spectra of the scalar variance and dissipation rate in $k_1$-direction are

$$E_{\theta 1}(k_1) = 2\int_{-\infty}^{\infty}\int_{-\infty}^{\infty} \phi_\theta(k_1,k_2,k_3)\, dk_2 dk_3 \tag{7}$$

$$D_{\theta 1}(k_1) = 3\nu_\theta \int_{-\infty}^{\infty}\int_{-\infty}^{\infty} k_1^2 \phi_\theta(k_1,k_2,k_3)\, dk_2 dk_3, \tag{8}$$

where the factor 3 in the latter equation is due to isotropy. Integration of (7) and (8) over $k_1$ yields the scalar variance and mean dissipation rate, respectively

$$\sigma_\theta = \int_0^\infty E_{\theta 1}(k_1)\, dk_1 \tag{9}$$

$$\varepsilon_\theta = \int_0^\infty D_{\theta 1}(k_1)\, dk_1. \tag{10}$$

The filtering effect of the probe can be estimated by replacing $\phi_\theta$ with $\phi_\theta^*$ in (7)–(8) and, therefore, in (9)–(10). In particular, the correction factors for the scalar variance and dissipation rate are defined as

$$R_\theta(\ell) = \frac{\sigma_\theta^*(\ell)}{\sigma_\theta} \tag{11}$$

$$R_\varepsilon(\ell) = \frac{\varepsilon_\theta^*(\ell)}{\varepsilon_\theta}. \tag{12}$$

Knowing (11)–(12), one can correct the data measured by a probe of length $\ell$.

In physical space, the mixed velocity-scalar derivative skewness is

$$S_{u\theta} = -\frac{\left\langle \left(\partial u_1/\partial x_1\right)\left(\partial\theta/\partial x_1\right)^2\right\rangle}{\left\langle \left(\partial u_1/\partial x_1\right)^2\right\rangle^{1/2}\left\langle \left(\partial\theta/\partial x_1\right)^2\right\rangle}, \tag{13}$$

($u_1$ is the velocity component in $x_1$-direction), while in spectral space (13) becomes [4]

$$S_{u\theta} = \frac{3}{30^{1/2}} \frac{\int_0^\infty k^2 T_\theta(k,t)\, dk}{\left[\int_0^\infty k^2 E(k,t)\, dk\right]^{1/2}\int_0^\infty k^2 E_\theta(k,t)\, dk}. \tag{14}$$

Here, $T_\theta(k,t)$ is the scalar transfer and $E(k,t)$ is the 3D kinetic energy spectrum of the velocity. In view of the experimental application of this analysis, it is convenient to express the transfer in terms of the scalar spectrum, using the spectral dynamical equation

$$\frac{\partial}{\partial t}E_\theta(k,t) = T_\theta(k,t) - 2\nu_\theta k^2 E_\theta(k,t). \tag{15}$$

Then, in order to assess the effect of the probe resolution on $S_{u\theta}$, (14) has to be rewritten in terms of 1D spectra, i.e.

$$S_{u\theta} = \frac{\frac{1}{2}\int_0^\infty k_1^2 \frac{\partial}{\partial t}E_{\theta 1}(k,t)\, dk_1 + \frac{7}{3}\nu_\theta \int_0^\infty k_1^4 E_{\theta 1}(k_1,t)\, dk_1}{\left[\int_0^\infty k_1^2 E_{11}(k_1,t)\, dk_1\right]^{1/2}\int_0^\infty k_1^2 E_{\theta 1}(k_1,t)\, dk_1}, \tag{16}$$

where $E_{11}$ is the 1D velocity spectrum. Finally, by considering the true and measured values of (16), the attenuation factor for the mixed skewness is defined as

$$R_S(\ell) = \frac{S_{u\theta}^*(\ell)}{S_{u\theta}}. \tag{17}$$

An approximate estimate of the mixed skewness can be obtained by neglecting the term $\partial E_\theta/\partial t$ in (15), i.e.

$$T_\theta(k,t) \simeq 2\nu_\theta k^2 E_\theta(k,t), \tag{18}$$

since one expects that such term will contribute mainly in the large scale range, especially at high $R_\lambda$; this approximation is commonly applied in experiments. In the following, the mixed skewness estimates that employ (18) are denoted by a prime.

Wyngaard [16] provided distributions of $R_\theta(\ell)$ and $R_\varepsilon(\ell)$ calculated via Pao's model [11] of the scalar 3D spectrum. Here, we reproduce similar results but using the scalar model spectrum of Kraichnan [8]

$$\frac{E_\theta(k\eta_B)}{\theta_B^2\eta_B} = q(k\eta_B)^{-1}\left(1+(6q)^{1/2}k\eta_B\right)\exp\left(-(6q)^{1/2}k\eta_B\right), \tag{19}$$

with $q = 2\sqrt{5}$ [12]. Eq. (19), is normalised by Batchelor scales $\eta_B, \theta_B (= \varepsilon_\theta^{1/2}/\gamma^{1/2}$, with $\gamma = \varepsilon^{1/2}/\nu^{1/2}$ the mean strain rate).

Finally, to calculate $S_{u\theta}$ and $S_{u\theta}^*$, a model spectrum for the velocity is needed. In this work, the expression

$$\frac{E(k\eta)}{u_K^2\eta} = (k\eta)^a \exp(-b(k\eta)) \tag{20}$$

($u_K = \nu^{1/4}\varepsilon^{1/4}$ is the Kolmogorov velocity) is considered, with $a = -5/3$ and $b = 5$. Recent numerical simulations performed at moderate $R_\lambda$ [4, 9] have shown that the models (19)–(20) can represent rather accurately the smallest turbulent scales.

#### Numerical Details

Homogeneous isotropic turbulence is simulated with a pseudo-spectral code which solves the Navier–Stokes equation in a periodic box. The transport-diffusion equation for a passive scalar at Schmidt number $Sc$ unity is also solved simultaneously. The computational domain is cubic, discretised by $256^3$ Fourier modes (more details about the numerical solution and initial conditions can be found in [7]). After the scalar is introduced, the velocity and scalar fields decay freely in time. The data used in the following correspond to a Taylor-microscale Reynolds number $R_\lambda = \sigma_{u_1}^{1/2}\lambda/\nu$ [$\sigma_{u_1}$ is the variance of $u_1$, $\lambda = (15\nu\sigma_{u_1}/\varepsilon)^{1/2}$ is the Taylor-microscale] of 42, while the turbulent Péclet number $Pe = \sigma_{u_1}^{1/2}\lambda_\theta/\nu_\theta$ [$\lambda_\theta = (3\nu_\theta\sigma_\theta/\varepsilon_\theta)^{1/2}$ is the Corrsin microscale] is 20. Although these values of $R_\lambda$ and $Pe$ are low, they are of the same order achieved in many laboratory experiments with grid turbulence [5].

For the resolution analysis, it is crucial that the simulated fields are fully resolved, down to the dissipative scale. This is verified, here, in different manners. First, the values of $k_{\max}\eta$ (and therefore $k_{\max}\eta_B$, since $Sc = 1$) are $\geq 2$, which ensures adequate resolution of the small scales for the velocity and the scalar. Also because of this constraint, the useful range of $R_\lambda$ is limited to low values. Second, it is checked that the spectra of the mean dissipation rate and of the second-order derivative vanish at large wavenumbers (see next section). Third, the values of $S_u$ and $S_{u\theta}$ are verified to be near 0.5, as expected for well-resolved fully developed turbulence [4]. The mixed skewness $S'_{u\theta}$ calculated in spectral space is 0.55, or 10% larger than $S_{u\theta}$ . This

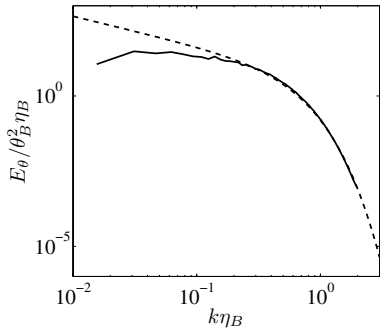


Figure 2: 3D spectra of the scalar variance, normalised by Batchelor scales. —, present DNS data; −−, Kraichnan model.

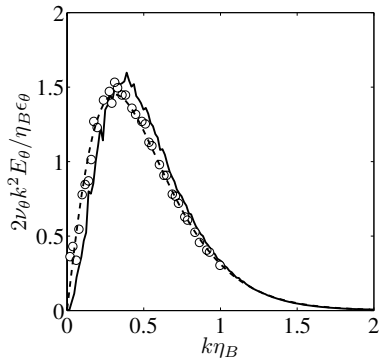


Figure 3: 3D spectra of the scalar dissipation rate, normalised by Batchelor scales. —, present DNS data; ◯, data from [14] at $Sc = 0.7$, $R_\lambda = 68.1$; −−, Kraichnan model.

highlights the fact that, although the term $\partial E_\theta/\partial t$ contributes mostly in the energy containing range, at the present value of $R_\lambda$ it does affect the estimate of the mixed skewness.

#### Results

The scalar spectrum from the DNS is plotted in figure 2, normalised by Batchelor scales. (Although, in the following, 1D spectra are used to estimate the attenuation factors, 3D distributions are reported initially, for comparison with data from the literature.) Kraichnan model spectrum, also plotted, agrees almost perfectly with the numerical data, at large wavenumbers. Scalar dissipation spectra are given in figure 3; here, the ordinate is normalised so that the integral of the curves is unity. The numerical distributions close at $k\eta_B \simeq 2$, lending confidence to the estimate of the dissipation rate. Further, the present data agree satisfactorily with those of [14], computed for only slightly different values of $Sc$ and $R_\lambda$. Also the distribution from the Kraichnan model follows accurately the numerical data. Spectral distributions of the second-order derivative are reported in figure 4. At large wavenumbers, near $k\eta_B \simeq 3$, the numerical data approach zero, hinting that the resolution is adequate for computing the mixed skewness (recall that the second-order derivative appears in the numerator of $S_{u\theta}$). The Kraichnan model and, more especially, the data from [2] at similar $R_\lambda$ (also reproduced in figure 4) do not differ significantly.

The filtering effect of the probe is estimated via (2), using different averaging lengths $\ell$, which are taken as multiples of the numerical grid spacing. Correction factors for $\sigma_\theta$ and $\varepsilon_\theta$ as a function of $\ell/\eta_B$ are given in figure 5. It is seen that $\varepsilon_\theta$ is attenuated the most: for $\ell/\eta_B \simeq 10$, the reduction is about 30%;

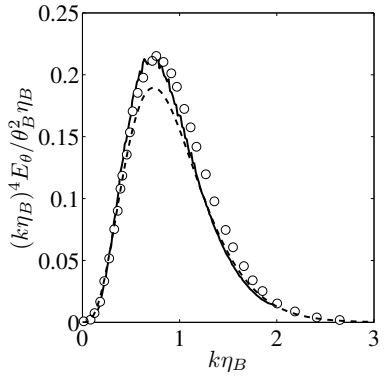


Figure 4: 3D spectra of the scalar second-order derivative, normalised by Batchelor scales. —, present DNS data; ◯, data from [2], $Sc = 1$, $R_\lambda \simeq 40$; −−, Kraichnan model.

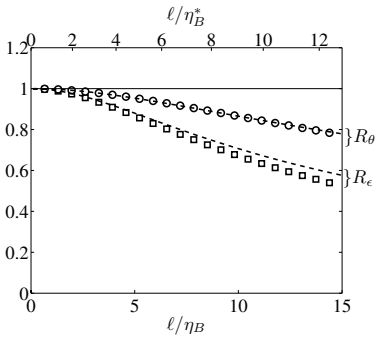


Figure 5: Attenuation factors for the scalar variance and mean dissipation rate. Symbols are for present DNS data: ◯, $R_\theta$; □, $R_\varepsilon$. Dashed lines are for the Kraichnan model. The horizontal scale on top is normalised by the Batchelor length scale $\eta_B^*$ as affected by the lack of resolution.

in general, the attenuation on $\theta$ is nearly half that on $\varepsilon$. The prediction for $R_\theta$ and $R_\varepsilon$ from the numerical data is close to that from Kraichnan model, despite the fact that the latter does not describe accurately the scalar spectrum at small $k_{\max}\eta_B$. This indicates that the large scales, which are more flow-dependent, need not be reproduced closely by the model. Note that the condition $k_{\max}\eta_B \simeq 1$, (corresponding to $\ell/\eta_B \simeq \pi$), often deemed adequate in experiments to guarantee resolution of the small scales, yields errors on $\varepsilon_\theta$ of nearly 10%.

Figure 6 shows the distributions of the mixed scalar attenuation. In evaluating (16), the time derivative of the scalar spectrum has been approximated by a finite difference. Unlike $R_\theta$ and $R_\varepsilon$, $R_S$ is $> 1$ and levels off near 1.15, for large $\ell/\eta_B$. Therefore, the mixed skewness is *overestimated*, when the measurements are underresolved. Further, since $R_S$ is almost independent on $\ell/\eta_B$, checking that the value of $S_{u\theta}$ is near 0.5 does not guarantee that good resolution has been achieved. The reason for the inappropriateness of $S_{u\theta}$ as a test for the resolution is related to its definition: the attenuation of the third-order moment in its numerator is balanced by the attenuation of the scalar and velocity derivatives in the denominator. This conclusion arguably applies also to numerical simulations having poor spatial resolution.

Figure 6 includes the mixed skewness calculated via the approximation (18). The values of $S'_{u\theta}$ are $< 1$, hence implying that the mixed skewness is underestimated, when the resolution is poor.

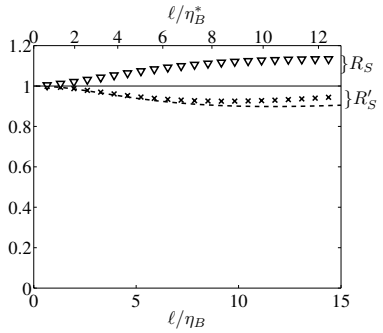


Figure 6: Attenuation factor for the mixed velocity-scalar derivative skewness. Symbols are for present DNS data: $\triangledown$, $R_S$; $\times$, $R'_S$. Dashed line is for the Kraichnan model.

A similar outcome is obtained when using (18) in combination with the spectral models. It can be concluded that the neglect of the $\partial E_\theta/\partial t$ term in (15) entails unacceptable errors, when estimating the effect of the resolution on the mixed skewness at small $R_\lambda$. However, it is expected that, as $R_\lambda$ increases, such approximation will be more fitting, because of the wider separation between large and small length scales. In figures 5 and 6, the second horizontal axis on top is normalised by the Batchelor length scale $\eta_B^* = R_\varepsilon^{-1/4}\eta_B$ as measured by a probe of size $\ell/\eta_B$, that is, taking into account the lack of resolution. This makes the curves readily usable by experimentalists.

#### Conclusions

The effect of finite sensor resolution on the measurement of scalar variance, scalar mean dissipation rate, and mixed velocity-scalar derivative skewness has been estimated. A DNS database for a passive scalar at Schmidt number unity, advected by isotropic turbulence at low Taylor-microscale Reynolds number, has been used for this purpose. Results for a sensor length in the range $0 < \ell/\eta_B < 15$ show that the variance and, more especially, the dissipation rate are underestimated, while the mixed skewness is overestimated. This latter is also found to be largely insensitive to the probe size, and therefore should not be used to assess the adequacy of the resolution. Correction factors derived from Kraichnan model spectrum are found to be close to the values provided by the DNS.

#### Acknowledgements

This work, conducted as part of the award (Modelling and simulation of turbulent conductive flows in the limit of low magnetic Reynolds number) made under the European Heads of Research Councils and European Science Foundation EURYI (European Young Investigator) Awards scheme, was supported by funds from the Participating Organisations of EURYI and the EC Sixth Framework Programme. Financial support from the Communauté Française de Belgique (ARC 02/07-283) and from the contract of association EURATOM-Belgian state is also gratefully acknowledged. The content of the publication is the sole responsibility of the authors and it does not necessarily represent the views of the Commission or its services. MK and DC are supported by FRS-FNRS Belgium.

#### References

[1] Antonia, R. A. and Mi, J., Corrections for velocity and temperature derivatives in turbulent flows, *Exp. Fluids*, **14**, 1993, 203–208.

[2] Antonia, R. A. and Orlandi, P., Similarity of decaying isotropic turbulence with a passive scalar, *J. Fluid Mech.*, **505**, 2004, 123–151.

[3] Antonia, R. A., Zhu, Y. and Kim, J., On the measurement of lateral velocity derivatives in turbulent flows, *Exp. Fluids*, **15**, 1993, 65–69.

[4] Bogucki, D., Domaradzki, J. A. and Yeung, P. K., Direct numerical simulations of passive scalars with $Pr > 1$ advected by turbulent flow, *J. Fluid Mech.*, **343**, 1997, 111–130.

[5] Burattini, P. and Antonia, R. A., The effect of different X-wire calibration schemes on some turbulence statistics, *Exp. Fluids*, **38**, 2005, 80–89.

[6] Burattini, P., Antonia, R. A. and Danaila, L., Similarity in the far field of a turbulent round jet, *Phys. Fluids*, **17**, 2005, 025101.

[7] Burattini, P., Kinet, M., Carati, D. and Knaepen, B., Corrections for underresolved scalar measurements in turbulent flows using a DNS database, *Exp. Fluids*, **43**, 2007, 31–37.

[8] Kraichnan, R. H., Small-scale structure of a scalar field convected by turbulence, *Phys. Fluids*, **11**, 1968, 945–953.

[9] Martinez, D. O., Chen, S., Doolen, G. D., Kraichnan, R. H., Wang, L.-P. and Zhou, Y., Energy spectrum in the dissipation range of fluid turbulence, *J. Plasma Phys.*, **57**, 1997, 195–201.

[10] Mi, J. and Nathan, G. J., The influence of probe resolution on the measurement of a passive scalar and its derivatives, *Exp. Fluids*, **34**, 2003, 687–696.

[11] Pao, Y.-H., Structure of turbulent velocity and scalar fields in large wavenumbers, *Phys. Fluids*, **8**, 1965, 1063–1075.

[12] Qian, J., Viscous range of turbulent scalar of large Prandtl number, *Fluid Dyn. Res.*, **15**, 1995, 103–112.

[13] Suzuki, Y. and Kasagi, N., Evaluation of hot-wire measurements in wall shear turbulence using a direct numerical simulation database, *Exp. Therm. Fluid Sci.*, **5**, 1992, 69–77.

[14] Wang, L.-P., Chen, S. and Brasseur, J. G., Examination of hypotheses in the Kolmogorov refined turbulence theory through high-resolution simulations. Part 2. Passive scalar field, *J. Fluid Mech.*, **400**, 1999, 163–197.

[15] Wyngaard, J. C., Measurement of small-scale turbulence structure with hot wires, *J. Phys. E: Sci. Instrum.*, **1**, 1968, 1105–1108.

[16] Wyngaard, J. C., Spatial resolution of a resistance wire temperature sensor, *Phys. Fluids*, **14**, 1971, 2052–2054.